Mesostructured ZnO/Au Nanoparticle Composites with Enhanced Photocatalytic Activity

Carina Bojer,[1+] Judith Schöbel,[2+] Thomas Martin,[1] Thomas Lunkenbein,[3] Daniel R. Wagner,[1] Andreas Greiner,[2,4] Josef Breu[1,4*] and Holger Schmalz[2,4*]

[1] Lehrstuhl für Anorganische Chemie I, Universität Bayreuth, 95440 Bayreuth, Germany

E-mail: josef.breu@uni-bayreuth.de

[2] Lehrstuhl für Makromolekulare Chemie II, Universität Bayreuth, 95440 Bayreuth, Germany

E-Mail: holger.schmalz@uni-bayreuth.de

[3] Abteilung für Anorganische Chemie, Fritz-Haber Institut der Max-Planck Gesellschaft, 14195 Berlin, Germany

[4] Bavarian Polymer Institute (BPI), Universität Bayreuth, 95440 Bayreuth, Germany

[+] C.B. and J.S. contributed equally to this work.

Dedicated to Axel H. E. Müller on the occasion of his 70th birthday.

Abstract

Ease of catalyst separation from reaction mixtures represents a significant advantage in heterogeneous photocatalytic wastewater treatment. However, the activity of the catalyst strongly depends on its surface-to-volume ratio. Here, we present an approach based on cylindrical polybutadiene-*block*-poly(2-vinylpyridine) polymer brushes as template, which can be simultaneously loaded with zinc oxide (ZnO) and gold (Au) nanoparticles. Pyrolytic template removal of the polymer yields in mesostructured ZnO/Au composites, showing higher efficiencies in the photocatalytic degradation of ciprofloxacin and levofloxacin (generic antibiotics present in clinical wastewater) as compared to neat mesostructured ZnO. Upscaling of the presented catalyst is straightforward promising high technical relevance.

Keywords

Mesostructure, cylindrical polymer brushes, wastewater treatment, photocatalyst, nanowires

1. Introduction

The removal of pharmaceuticals from clinical wastewater is a burning issue in environmental science. Efficient removal of active drugs like, antibiotics, cytostatics, beta-blockers or antiphlogistics, is required before treatment by standard biological purification techniques in sewage plants.[1–5] For instance, ciprofloxacin, a widely employed antibiotic from the fluoroquinolone group, is problematic due to its gentoxicity.[6,7] Consequently, high stability, low biodegradability and toxicity of these active agents limit the use of mild biological degradation processes and there is a demand for chemical oxidation.[8] Advanced oxidation processes (AOP), which are based on the formation of highly reactive hydroxyl radicals, provide promising results in the catalytic degradation of organic pollutants. In particular, photocatalytic AOPs are of special interest, as in addition to UV light only a transition metal oxide catalyst, e.g. titanium dioxide (TiO_2) or zinc oxide (ZnO), is needed.[9–11] If solar energy, consisting of UV and visible light, is applied to the catalyst, an enhancement of the activity by doping the transition metal oxide with noble metal nanoparticles (NPs), e.g., gold, platinum or silver, has been observed. This effect is attributed to the localized surface plasmon resonance of the noble metal NPs, which causes an increased absorption of visible light and a charge-transfer to the transition metal oxide.[12–15]

With respect to clinical wastewater (typical pH = 8), the catalyst has to fulfil different requirements.[16,17] Most pharmaceuticals are rendered soluble in body fluids by deprotonated carboxylic acid groups. For ciprofloxacin the isoelectric point of the zwitterion is at a pH value of 7.4.[18] Thus, a catalyst bearing a positive surface charge at a pH of 8 is advantageous, as this will enhance the electrostatic interactions between antibiotic and catalyst. Previous studies showed that in contrast to Degussa P25, a TiO_2 catalyst with its point of zero charge (PZC) at a pH of 6.9, ZnO fulfils this requirement as its PZC is 9.2.[19,20] Another important criterion for increasing catalytic activity is the accessible surface area of the catalyst. Using nanomaterials, like nanoparticles, -tubes, or -wires, the active surface can be maximized due to their high surface-to-volume ratio, resulting in an increased performance for example in environmental remediation.[4] However, the reusability of NP catalysts is limited due to the inherently difficult separation of NPs from a fluid reaction media. Applying polymer templates for the controlled assembly of NPs into mesostructured hybrid materials represents a good compromise between preserving a high accessible surface area while allowing for filtration of the catalyst (Scheme 1). In particular, cylindrical polymer brushes (CPBs) proved to be promising template materials, as their composition and functionality can be tailored to meet the demands for an efficient mesostructuring of NPs.[21–24] As shown with different transition metal oxides, like TiO_2 or WO_3, these supports are able to prevent segregation and, therefore, a loss of surface area.[25–27] Pyrolytic removal of the polymeric template leads to mesostructured one-dimensional aggregates where adjacent NPs become connected *via* necks during sintering. [28,29] The resulting nonwoven structures provide sufficient mechanical stability to be used in continuous flow cells, while at the same time offering a high accessible surface area.[30]

Herein, we report the synthesis of mesostructured ZnO/Au NP composites for the efficient detoxification of hospital wastewater, exemplified on the photocatalytic degradation of ciprofloxacin and levofloxacin. To this end, cationic CPBs, consisting of a cross-linked polybutadiene (PB) core and a quaternized poly(2-vinylpyridine) (P2VP) corona, were used as template for the simultaneous mesostructuring of ZnO and Au NPs. Pyrolytic removal of the polymeric template leads to hierarchically structured nonwovens composed of catalytically active ZnO/Au nanowires (Scheme 1).

Scheme 1. Self-assembly of a BV diblock copolymer (A) results in a cylindrical bulk morphology with hexagonally packed PB cylinders in a P2VP matrix (B). Crosslinking the PB cylinders and quaternization of the P2VP corona blocks produces cationic CPBs (C). These CPBs are used as templates for the simultaneous loading with ZnO and Au NPs (D). The resulting hybrid (E) is transformed into a mesostructured nonwoven (F) consisting of ZnO/Au nanowires by calcination.

2. Experimental Part

2.1 Chemicals

All chemicals were purchased from Sigma-Aldrich (Germany) and used as received if not otherwise noted.

2.2 Synthesis of the BV diblock copolymer

The polybutadiene-*block*-poly(2-vinylpyridine) (BV) diblock copolymer was synthesized by sequential living anionic polymerization in THF with *sec*-butyllithium as initiator, as published elsewhere.[28] The molecular weight and the composition of the BV diblock copolymer were determined by a combination of ^{1}H-NMR spectroscopy (Bruker Ultrashield AC300) and MALDI-TOF MS (Bruker Reflex III) and resulted in $B_{19}V_{81}^{60}$ (subscripts denote the mass fraction of the corresponding block in wt-% and the superscript gives the overall molecular weight in kg mol^{-1}). The molar mass dispersity of the BV diblock copolymer was determined by THF-SEC to $Đ_M$ = 1.02.

2.3 Formation of the cationic CPB template

Typically, 1 g of a $B_{19}V_{81}^{60}$ film with 0.1 g of the photoinitiator Lucirin TPO (BASF) was prepared by solvent-casting from chloroform. The resulting hexagonally ordered film was crosslinked using a UV hand lamp (Hoenle, 2 h per side). The crosslinked $B_{19}V_{81}^{60}$ film was dissolved in 200 mL chloroform and 3 mL of an iodomethane solution (99 %) was added dropwise for quaternization of the poly(2-vinylpyridine) (P2VP) block. The solvent and the iodomethane solution were allowed to evaporate. The quaternized product (BV_q) was washed with pentane, dissolved in water and freeze-dried.

2.4 Synthesis of the hybrid material and calcination

As an example, for the synthesis of the ZnO/Au_12 hybrid material 200 mg of BV_q was dissolved in 200 mL DMSO. To this solution, 6 mL of tetrachloroauric acid trihydrate (Alfa Aesar, 0.1 M in THF) was added. Subsequently, 3 mL of a sodium borohydride solution (1 M in deionized water) was added and the colour changed to deep purple. Immediately, 125 mL of an acetate-stabilized ZnO NP dispersion (6.9 g L^{-1} in ethanol, synthesis reported in Ref. 30) was added. The reaction mixture was stirred for 10 min. The purple precipitate was isolated by centrifugation (3 min, 7000 rpm) and washed 5 times with ethanol and one time with deionized water and then freeze-dried. The details of all synthesized materials are summarized in Table S1. Heat treatment at 490 °C for 5 min in a tube furnace (heating/cooling rate 180 K h^{-1}) under air lead to the removal of the organic CPB template and sintering into an all-inorganic nonwoven composite structure.

2.5 Photocatalytic degradation

Photocatalytic degradation of anionic antibiotics (ciprofloxacin and levofloxacin) was realized in a self-constructed continuous flow reactor (Scheme S1). The synthesized ZnO/Au nanowire photocatalyst (15 mg) was drop coated on a glass microfiber filter (Whatman, 37 mm diameter) and 400 mL of the ciprofloxacin or levofloxacin solution ($c = 2 \cdot 10^{-5}$ mol L^{-1}, pH = 8 (borate/HCl buffer, Titrisol)) was circulated at a flow rate of 12 L h^{-1}. The degradation with solar spectrum (300 W Xenon lamp, AM1.5 filter, 1000 W m^{-2}) was monitored using UV-Vis spectroscopy (samples taken every 5-15 min). The experiments were done without catalyst as a reference, with Degussa P25, ZnO nanotubes and ZnO/Au nanowire composites with different ZnO/Au ratios. All catalysts were tested at least three times to guarantee reproducible results.

2.6 Instruments

Powder X-ray diffraction (PXRD) measurements were done using a STOE Stadi P diffractometer. $CuK_{\alpha 1}$ radiation and a Mythen 1K silicon strip-detector were used. Rietveld analysis was done with TOPAS Academic (fundamental parameters approach for profile fitting). The crystallite sizes were determined using implemented macros (elliptical particles) and the composition was estimated using quantitative Rietveld-refinement.

Transmission electron microscopy (TEM) micrographs were acquired using a Zeiss 922 Omega EFTEM (Zeiss NTS GmbH, Oberkochen, Germany), operating at an accelerating voltage of 200 kV. Zero-loss filtered images were taken with a bottom-mounted CCD camera system (Ultrascan 1000, Gatan). The micrographs were processed by the digital imaging processing software Gatan Digital Micrograph 3.9 for GMS 1.4. The samples were prepared by drop-coating of dilute dispersions of the hybrid materials/composites in ethanol (c = 0.1 g L^{-1}) onto carbon-coated copper grids, followed by blotting with a filter paper.

High resolution TEM and local energy dispersive X-ray (EDX) maps were recorded on a double corrected JEOL ARM-200CF equipped with a high angle Silicon Drift EDX detector with a solid angle of up to 0.98 sterradians.

Scanning electron microscopy (SEM) images and energy dispersive X-ray analysis (EDX) data were obtained with a LEO 1530 FESEM scanning electron microscope equipped with a field emission cathode.

A Quantachrome Autosorb 1 was used to determine the surface area with N_2 at 77 K after degassing the sample at 363 K for 12 h.

UV-Vis absorption spectra were measured with a Varian Cary 300 spectrometer using Hellma precision cells made of Quartz SUPRASIL (type 100-QS, light path 10 mm).

Thermal gravimetric analysis (TGA) was performed on a Netzsch TG 209F1 Libra under synthetic air. The samples were heated from 25-800 °C at a heating rate of 10 K min^{-1}.

The PZC was determined using a ParticleMetrix StabiSizer PMX 200C. 50 mg catalyst in 10 mL water with a pH of 10.5 (adjusted with 0.01 M NaOH) were titrated with 0.05 M HCl until the streaming potential was zero.

3. Results and Discussion

3.1 Formation of cylindrical ZnO/Au hybrids

ZnO/Au hybrids were prepared by employing cationic CPBs as template for the simultaneous loading with Au and ZnO NPs (Scheme 1). The cationic CPBs were obtained from a polybutadiene-*block*-poly(2-vinylpyridine) (BV) diblock copolymer ($B_{19}V_{81}^{60}$: subscripts denote the mass fraction of the corresponding block in wt-% and the superscript gives the molecular weight in kg mol^{-1}), which forms a bulk morphology with hexagonally arranged PB cylinders embedded in a P2VP matrix (Scheme 1A, B). Subsequent photo-crosslinking of the PB cylinders followed by dissolution and quaternization of the P2VP block resulted in the desired CPBs with a positively charged corona (Scheme 1C). The Au NPs were generated *in-situ* by reduction of tetrachloroauric acid trihydrate and as a ZnO source phase pure, acetate-stabilized ZnO NPs with a number-weighted hydrodynamic diameter of D_h = 3.2 nm were used (Scheme 1D, E; Table S1). Details on the synthesis and characterization of the used monodisperse ZnO NPs can be found elsewhere.[30] To investigate the effect of the Au content on the photocatalytic degradation of antibiotics (ciprofloxacin and levofloxacin), four different ZnO/Au hybrid materials (8 , 12 , 15 and 26 wt-% Au with respect to the overall amount of inorganic material in the hybrid) were synthesized. The notation ZnO/Au_x, with x denoting the Au content in wt-%, will be used in the following. The total amount of ZnO and Au immobilized by the cationic CPB template was determined by TGA measurements to 74-79 wt-% (Fig. S1). This is in good agreement with the employed amounts of the CPB template, ZnO NP and Au precursor in the synthesis of the hybrid materials (80 wt-% CPB template).

The TEM micrographs of the obtained hybrids reveal the controlled co-assembly of ZnO and Au NPs under preservation of the cylindrical structure of the cationic CPB template (Fig. 1). The cylindrical PB core of the CPB template can be clearly identified in the corresponding greyscale analysis for the ZnO/Au_12 hybrid, shown in the inset of Fig. 1B.

Fig. 1. TEM images of the ZnO/Au_8 (A), ZnO/Au_12 (B; inset in B: grey scale analysis), ZnO/Au_15 (C) and the ZnO/Au_26 hybrid materials (D).

3.2 Formation of ZnO/Au composite nanowires

ZnO/Au composite nanowires were obtained by pyrolysis of the ZnO/Au hybrid cylinders in air at 490 °C. After template removal, the one-dimensional structure of the CPB template was retained, resulting in the formation of mesostructured ZnO/Au composite nonwovens (Fig. 2A-D). Only for the ZnO/Au_26 nonwoven a partial agglomeration of the hybrid cylinders upon calcination can be observed. The composition of the obtained ZnO/Au nanowires was determined by EDX measurements (Table S2) and is in good agreement with the used amount of educts. Elemental analysis (Table S3) and TGA measurements (Fig. S1) confirm the absence of organic material after pyrolysis (less than 0.2 %), indicating the complete removal of the organic CPB template. The mesostructured nonwovens show high specific surface areas of 25 - 48 m^2g^{-1}, as determined by nitrogen physisorption (Fig. S2, Table S4). The high-angle annular dark-field scanning transmission electron microscopy (HAADF-STEM) image of ZnO/Au_12 nanowires (Fig. 2E) confirms the retention of the wire-like mesostructure. In HAADF-STEM the contrast is due to Rutherford scattering, which is almost proportional to Z^2. Thus, Au (bright) and ZnO (grey) moieties are directly

distinguishable and can further be identified by an energy dispersive X-ray (EDX) map of the same particles (Fig. 2E, inset). The HAADF-STEM image reveals a partial wetting of the Au NPs on top of the ZnO nanocrystals, thus, increasing the Au/ZnO perimeter. In addition, the HR-TEM image in Fig. 3F highlights a representative mesostructure of the nanowires, which is composed of randomly oriented, individual ZnO nanocrystals that form intraparticular mesopores. Those intraparticular mesopores may ensure a higher mass transport in the photocatalytic liquid phase detoxification reaction. Moreover, the ZnO nanowires are partially decorated by isolated Au nanoparticles.

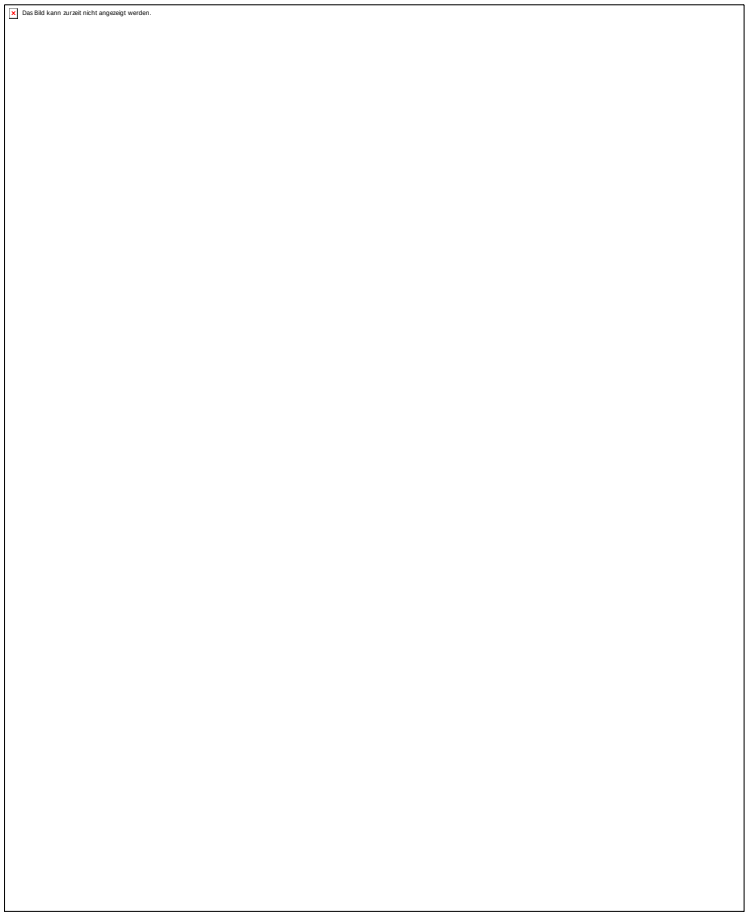

Fig. 2. SEM images of ZnO/Au_8 (A), ZnO/Au_12 (B), ZnO/Au_15 (C) and ZnO/Au_26 nanowires (D). HAADF-STEM image of ZnO/Au_12 nanowires (E, inset: EDX map of the same particle; white – ZnO; red – Au). HR-TEM image of ZnO/Au_12 nanowires (F); the inset denotes the Fast Fourier Transform (FFT) of the region that is labelled with Au.

In order to get a closer insight into the calcination process and its impact on the Au and ZnO NP sizes, the morphological changes for the ZnO/Au_12 and ZnO/Au_26 hybrid cylinders upon calcination were studied by PXRD (Fig. 3A, B). The PXRD data show a halo in the range of $2q = 20\text{-}30°$, which is characteristic for the amorphous CPB template. The crystalline reflections of the hybrid materials can be assigned to ZnO and Au, respectively. For ZnO/Au_12 Rietveld refinement yields average coherent scattering domains of

3.4(2) x 3.7(2) nm for ZnO and 3.5(2) x 4.9(2) nm for Au, respectively (Fig. S3, Table S5). For ZnO/Au_26 domain sizes of 3.5(2) x 4.4(3) nm for ZnO and 3.7(6) x 5.3(4) nm for Au (Fig. S4 and Table S6) were obtained.

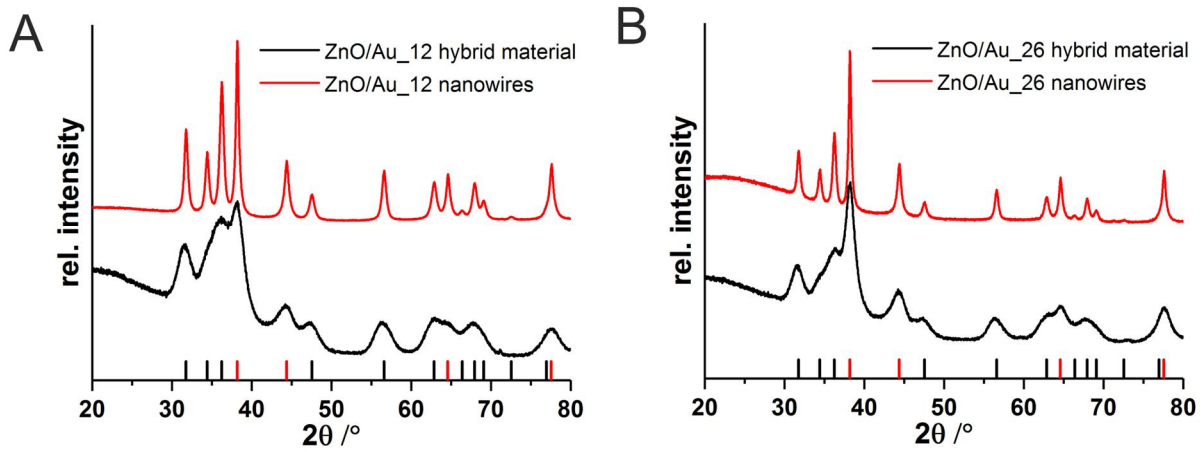

Fig. 3. PXRD patterns of ZnO/Au_12 (A) and ZnO/Au_26 (B) hybrid cylinders and nanowires with the reference cards of ZnO (black ticks PDF-Nr.: 00-036-145) and Au (red ticks PDF-Nr.: 00-004-0784).

The decrease of the full width at half maxima of PXRD peaks (ZnO/Au_12, Fig. 3A; ZnO/Au_26, Fig. 3B) indicates Ostwald ripening upon pyrolysis. For ZnO/Au_12 Rietveld analysis confirms the growth to a crystallite size of 12.5(4) x 15.5(4) nm for ZnO and 17.5(4) x 24.4(5) nm for Au, respectively (Fig. S5 and Table S7). A similar trend is observed for ZnO/Au_26, showing increased crystallite sizes of 14.5(8) x 16.9(8) for ZnO and 16.9(3) x 23.7(5) for Au (Fig. S6 and Table S8). The composition of the calcinated ZnO/Au_12 and ZnO/Au_26 composites is confirmed by Rietveld analysis and is in good agreement with the educt stoichiometry (12 wt-% Au and 26 wt-% Au, respectively) and EDX measurements (Table S2).

3.3 Photocatalytic degradation of negatively charged antibiotics

The photocatalytic degradation of ciprofloxacin and levofloxacin (isoelectric points (zwitterion): 7.4 and 6.8, respectively)[18], applying the ZnO/Au composite nanowires as catalysts, was studied using a continuous flow reactor. For comparative studies, neat ZnO nanotubes and Degussa P25 (TiO_2 based photocatalyst) were used. In the continuous flow reactor, 3.5 ppm of the catalyst material (with respect to ciprofloxacin or levofloxacin) was placed onto a filter paper to guarantee a homogeneous flow and the photocatalytic degradation of the two antibiotics was monitored at pH = 8 for 120 min applying terrestrial solar spectrum. No significant degradation was observed in the absence of a catalyst (Fig. S7A). The ZnO/Au_12 composite nanowires revealed the highest efficiency in the photocatalytic degradation of ciprofloxacin with a degradation of 16% in 120 min (Fig. 4A). For composite nanowires with a lower (8 wt-%) as well as higher (15 and 26 wt-%) Au content a significantly lower conversion was observed. Similar results were obtained for the degradation of levofloxacin (Fig. S8A), i.e., the ZnO/Au_12 composite nanowires showed the highest efficiency in photocatalytic degradation within the tested catalysts. The inferior behaviour for higher Au-loading can be attributed to electron-hole recombination centres, which limit the synergistic effect of the ZnO/Au composite.[31] The reduced performance of ZnO/Au_15 and ZnO/Au_26 also indicates that thermal effects due to the strong localized surface plasmon resonance absorption of Au NPs can be neglected, as in this case a higher activity would be expected for composites with higher Au contents. In comparison to previous studies on the degradation of ciprofloxacin with neat ZnO nanotubes,[30] the ZnO/Au_12 composite material shows a ca. 40% improved performance, as with the ZnO nanotubes a conversion of only 12% could be achieved under identical reaction conditions (Fig. S7A). A similar effect was observed for the photocatalytic degradation of levofloxacin (Fig. S8A).

The photocatalytic activity of the ZnO/Au_12 nanowires in the degradation of ciprofloxacin is moreover significantly improved with respect to Degussa P25, a commercial TiO_2 based photocatalyst (Fig. S7A). The advantage of ZnO/Au nanowire composites (PZC: 8.8) over Degussa P25 (PZC: 6.9)[19, 20] can be attributed to the opposite surface charge of ZnO based catalysts and ciprofloxacin (isoelectric point (zwitterion): 7.4)[18] at pH = 8 that favours drug adsorption on the catalyst surface. Any influence attributed to differences in the specific surface area of the catalysts can be ruled out, as the ZnO/Au_12 catalyst, showing the highest activity, exhibits the lowest specific surface area (25 $m^2 g^{-1}$, Table S4).

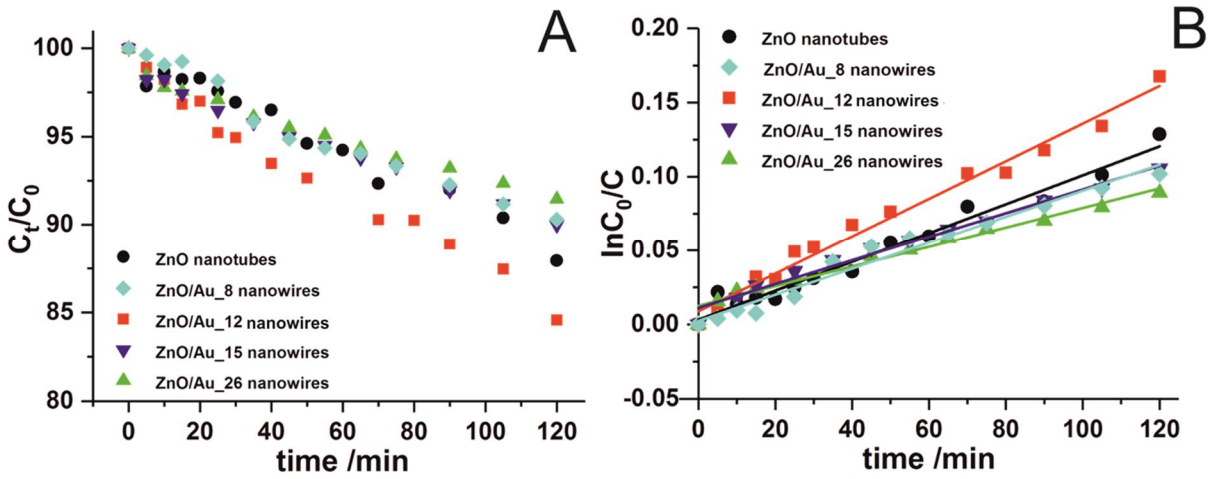

Fig. 4. Time-dependent decrease of ciprofloxacin concentration during irradiation with terrestrial solar spectrum (A) and corresponding first-order kinetics plots (B) for ZnO nanotubes and ZnO/Au composite nanowires.

As the photocatalytic degradation of ciprofloxacin using a ZnO or TiO_2 based catalyst already showed, this reaction follows a pseudo first-order kinetics and the apparent rate constants *k*' can be calculated from the slope of the corresponding first-order kinetics plot (Fig. 4B). The *k*' value for ZnO/Au_12 nanowires is $1.3 \cdot 10^{-3}$ min^{-1}. Compared with the *k'* value of neat ZnO nanotubes (*k*' = $9.6 \cdot 10^{-4}$ min^{-1}) the ZnO/Au_12 catalyst is 1.4 times faster. With reference to previous results, the ciprofloxacin degradation with ZnO/Au_12 nanowires is 3.7 times faster as compared to the standard Degussa P25 (Fig. S7B, Table S9). In case of levofloxacin, a 1.6 times faster degradation was observed for ZnO/Au_12 nanowires (Fig. S8B, Table S10). Conseqeuently, combining the electrostatically favoured adsorption of the antibiotics on the positively charged ZnO surface with the enhancement of Au NPs in mesostructured ZnO/Au_12 nonwovens has a distinct synergistic effect on the photocatalytic degradation. This results in an increase in degradation rate of about 40% for ciprofloxacin and 60% for levofloxacin, respectively, compared to neat ZnO nanotubes.

4. Conclusion

In this study, we used cationic CPBs as template for mesostructuring two different types of NPs with the aim of taking advantage of synergistic effects for the photocatalytic degradation of antibiotics in wastewater. ZnO and Au NPs were assembled simultaneously in a random fashion on cationic CPBs, resulting in mesostructured, nonwoven-like networks of ZnO/Au nanowires after pyrolytic template removal. The ZnO/Au nanowires with 12 wt-% Au show a significantly enhanced efficiency in the photocatalytic degradation of ciprofloxacin and levofloxacin with terrestrial solar spectrum, both with respect to neat ZnO nanotubes and

Degussa P25 NPs, respectively. This can be ascribed to the improved adsorption of the antibiotics, which are negatively charged at the slightly basic pH of hospital wastewater, on the positively charged ZnO surface combined with the enhancement due to the localized surface plasmon resonance of the Au NPs. The assembly of different types of NPs allows not only the synthesis of tailor-made catalyst systems for photocatalytical processes, but can also be transferred to other NP combinations with interesting catalytic properties. The non-woven structure of the catalyst ensures an easy recovery from the fluid reaction medium and, thus, excellent reusability, making this system highly interesting for technical applications.

Acknowledgement

This work was funded by the Collaborative Research Centre (SFB) 840. The authors thank Professor R. Schlögl (Fritz-Haber-Institute, Berlin) for access to HR-TEM. We appreciate the support of the Keylab for Optical and Electron Microscopy of the Bavarian Polymer Institute (BPI). J.S. acknowledges support by the Graduate School of the University of Bayreuth.

References

[1] N.M. Vieno, H. Härkki, T. Tuhkanen, L. Kronberg, Occurrence of Pharmaceuticals in River Water and Their Elimination in a Pilot-Scale Drinking Water Treatment Plant, Environ. Sci. Technol. 41 (2007) 5077–5084.

[2] E. Carraro, S. Bonetta, C. Bertino, E. Lorenzi, S. Bonetta, G. Gilli, Hospital Effluents Management: Chemical, Physical, Microbiological Risks and Legislation in Different Countries, J. Environ. Manage. 168 (2016) 185–199.

[3] J. Rivera-Utrilla, M. Sánchez-Polo, M.Á. Ferro-García, G. Prados-Joya, R. Ocampo-Pérez, Pharmaceuticals as Emerging Contaminants and their Removal from Water. A Review, Chemosphere 93 (2013) 1268–1287.

[4] M.M. Khin, A.S. Nair, V.J. Babu, R. Murugan, S. Ramakrishna, F. Yinjun, L. Junkang, C.W. Zhou, J. Choi, J. Paek, K. Lee, Y.S. Lee, D.H. Jeong, M.H. Cho, A Review on Nanomaterials for Environmental Remediation, Energy Environ. Sci. 5 (2012) 8075-819.

[5] A. Alsbaiee, B.J. Smith, L. Xiao, Y. Ling, D.E. Helbling, W.R. Dichtel, Rapid Removal of Organic Micropollutants from Water by a Porous β-Cyclodextrin Polymer, Nature 529 (2016) 190-194.

[6] D.G.J. Larsson, C. de Pedro, N. Paxeus, Effluent from Drug Manufactures Contains Extremely High Levels of Pharmaceuticals, J. Hazard. Mater. 148 (2007) 751–755.

[7] J.W. Beaber, B. Hochhut, M.K. Waldor, SOS Response Promotes Horizontal Dissemination of Antibiotic Resistance Genes, Nature 427 (2004) 72–74.

[8] A. Cincinelli, T. Martellini, E. Coppini, D. Fibbi, A. Katsoyiannis, Nanotechnologies for Removal of Pharmaceuticals and Personal Care Products from Water and Wastewater. A Review, J. Nanosci. Nanotechnol. 15 (2015) 3333–3347.

[9] U.I. Gaya, A.H. Abdullah, Heterogeneous Photocatalytic Degradation of Organic Contaminants over Titanium Dioxide: A Review of Fundamentals, Progress and

Problems, J. Photochem. Photobiol. C 9 (2008) 1–12.

[10] N.S. Lewis, Toward Cost-Effective Solar Energy Use, Science 315 (2007) 798–801.

[11] K.M. Lee, C.W. Lai, K.S. Ngai, J.C. Juan, Recent Developments of Zinc Oxide Based Photocatalyst in Water Treatment Technology: A Review, Water Res. 88 (2016) 428–448.

[12] R. Georgekutty, M.K. Seery, S.C. Pillai, A Highly Efficient Ag-ZnO Photocatalyst: Synthesis, Properties, and Mechanism, J. Phys. Chem. C 112 (2008) 13563–13570.

[13] A. Primo, A. Corma, H. García, Titania Supported Gold Nanoparticles as Photocatalyst, Phys. Chem. Chem. Phys. 13 (2011) 886–910.

[14] D. Tsukamoto, Y. Shiraishi, Y. Sugano, S. Ichikawa, S. Tanaka, T. Hirai, Gold Nanoparticles Located at the Interface of Anatase/Rutile TiO_2 Particles as Active Plasmonic Photocatalysts for Aerobic Oxidation, J. Am. Chem. Soc. 134 (2012) 6309–6315.

[15] R.M. Mohamed, D. McKinney, M.W. Kadi, I.A. Mkhalid, W. Sigmund, Platinum/Zinc Oxide Nanoparticles: Enhanced Photocatalysts Degrade Malachite Green Dye Under Visible Light Conditions, Ceram. Int. 42 (2016) 9375–9381.

[16] S. Gartiser, L. Brinker, T. Erbe, K. Kümmerer, R. Willmund, Belastung von Krankenhausabwasser mit gefährlichen Stoffen im Sinne § 7a WHG, Acta Hydroch. Hydrob. 24 (1996) 90–97.

[17] C. Boillot, C. Bazin, F. Tissot-Guerraz, J. Droguet, M. Perraud, J.C. Cetre, D. Trepo, Y. Perrodin, Daily Physicochemical, Microbiological and Ecotoxicological Fluctuations of a Hospital Effluent According to Technical and Care Activities, Sci. Total Environ. 403 (2008) 113–129.

[18] A. Dalhoff, S. Schubert, A. Vente, Pharmacodynamics of Finafloxacin, Ciprofloxacin, and Levofloxacin in Serum and Urine against TEM- and SHV-Type Extended-Spectrum-β-Lactamase-Producing Enterobacteriaceae Isolates from Patients with Urinary Tract Infections, Antimicrob. Agents Chemother. 61 (2017) e02446-16.

[19] M. Kosmulski, pH-Dependent Surface Charging and Points of Zero Charge II. Update, J. Colloid Interface Sci. 275 (2004) 214–224.

[20] M. Kosmulski, pH-Dependent Surface Charging and Points of Zero Charge, J. Colloid Interface Sci. 298 (2006) 730–741.

[21] M. Müllner, A.H.E. Müller, Cylindrical Polymer Brushes - Anisotropic Building Blocks, Unimolecular Templates and Particulate Nanocarriers, Polymer 98 (2016) 389–401.

[22] J. Yuan, Y. Xu, A. Walther, S. Bolisetty, M. Schumacher, H. Schmalz, M. Ballauff, A.H.E. Müller, Water-Soluble Organo-Silica Hybrid Nanowires, Nat. Mater. 7 (2008) 718–722.

[23] Y. Xu, J. Yuan, B. Fang, M. Drechsler, M. Müllner, S. Bolisetty, M. Ballauff, A.H.E. Müller, Hybrids of Magnetic Nanoparticles with Double-Hydrophilic Core/Shell Cylindrical Polymer Brushes and Their Alignment in a Magnetic Field, Adv. Funct. Mater. 20 (2010) 4182–4189.

[24] S.S. Sheiko, B.S. Sumerlin, K. Matyjaszewski, Cylindrical Molecular Brushes: Synthesis, Characterization and Properties, Prog. Polym. Sci. 33 (2008) 759–785.

[25] M. Müllner, T. Lunkenbein, N. Miyajima, J. Breu, A.H.E. Müller, A Facile Polymer Templating Route Toward High-Aspect-Ratio Crystalline Titania Nanostructures, Small 8 (2012) 2636–2640.

[26] M. Müllner, T. Lunkenbein, M. Schieder, A.H. Gröschel, N. Miyajima, M. Förtsch, J. Breu, F. Caruso, A.H.E. Müller, Template-Directed Mild Synthesis of Anatase Hybrid Nanotubes within Cylindrical Core-Shell-Corona Polymer Brushes, Macromolecules 45 (2012) 6981–6988.

[27] M. Schieder, T. Lunkenbein, T. Martin, W. Milius, G. Auffermann, J. Breu, Hierarchically Porous Tungsten Oxide Nanotubes with Crystalline Walls Made of the Metastable Orthorhombic Polymorph, J. Mater. Chem. A 1 (2013) 381–387.

[28] T. Lunkenbein, D. Rosenthal, T. Otremba, F. Girgsdies, Z. Li, H. Sai, C. Bojer, G. Auffermann, U. Wiesner, J. Breu, Access to Ordered Porous Molybdenum Oxycarbide/Carbon Nanocomposites, Angew. Chem. Int. Ed. 51 (2012) 12892–12896.

[29] M. Schieder, C. Bojer, J. vom Stein, S. Koch, T. Martin, H. Schmalz, J. Breu, T. Lunkenbein, Template Removal via Boudouard Equilibrium Allows for Synthesis of Mesostructured Molybdenum Compounds, Angew. Chem. Int. Ed. (2017), DOI: 10.1002/anie.201610786.

[30] C. Bojer, J. Schöbel, T. Martin, M. Ertl, H. Schmalz, J. Breu, Clinical Wastewater Treatment: Photochemical Removal of an Anionic Antibiotic (Ciprofloxacin) by Mesostructured High Aspect Ratio ZnO Nanotubes, Appl. Catal. B Environ. 204 (2017) 561–565.

[31] L. Sun, D. Zhao, Z. Song, C. Shan, Z. Zhang, B. Li, D. Shen, Gold Nanoparticles Modified ZnO Nanorods with Improved Photocatalytic Activity, J. Colloid Interface Sci. 363 (2011) 175–181.